Crystal Structures and Physicochemical Properties of Four New Lamotrigine Multicomponent Forms

ARTICLE *in* CRYSTAL GROWTH & DESIGN · JANUARY 2013

Impact Factor: 4.89 · DOI: 10.1021/cg301556j

CRYSTAL GROWTH & DESIGN

Article

pubs.acs.org/crystal

Crystal Structures and Physicochemical Properties of Four New Lamotrigine Multicomponent Forms

Renu Chadha,*[,†] Anupam Saini,[†] Sadhika Khullar,[‡] Dharamvir Singh Jain,[§] Sanjay K. Mandal,*[,‡] and T. N. Guru Row[∥]

[†]University Institute of Pharmaceutical Sciences, Panjab University, Chandigarh-160014, India

[‡]Department of Chemical Sciences, Indian Institute of Science Education and Research, Mohali, Sector 81, Manauli PO, S.A.S. Nagar, Mohali (Punjab) 140306, India

[§]Department of Chemistry, Panjab University, Chandigarh-160014, India

[∥]Solid State and Structural Chemistry Unit (SSCU), Indian Institute of Science, Bangalore-560012, India

Supporting Information

ABSTRACT: In the present study, four new multicomponent forms of lamotrigine (LTG) with selected carboxylic acids, viz. acetic acid, propionic acid, sorbic acid, and glutaric acid, have been identified. Preliminary solid-state characterization was done by differential scanning calorimetry/thermogravimetric, infrared, and powder X-ray diffraction techniques. X-ray single-crystal structure analysis confirmed the proton transfer, stoichiometry, and the molecular composition, revealing all of these to be a new salt/salt-cocrystal/salt monosolvate monohydrate of LTG. All four compounds exhibited both the aminopyridine dimer of LTG (motif 4) and cation−anion dimers between protonated LTG and the carboxylate anion in their crystal structures. Further, these new crystal forms were subjected to solubility studies in water, powder dissolution studies in 0.1 N HCl, and stability studies under humid conditions in comparison with pure LTG base. The solubility of these compounds in water is significantly enhanced compared with that of pure base, which is attributed to the type of packing motifs present in their crystal structures as well as to the lowering of the pH by the acidic coformers. Solid residues of all forms remaining after solubility and dissolution experiments were also assessed for any transformation in water and acidic medium.

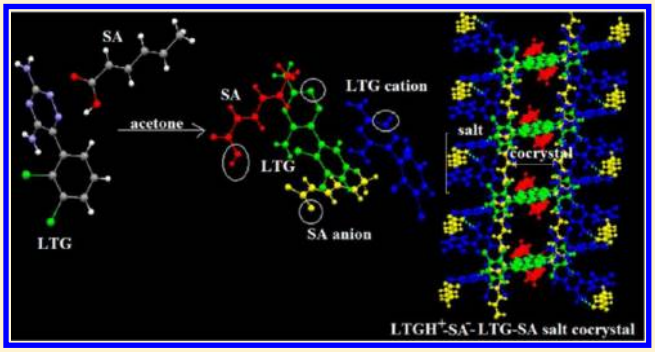

INTRODUCTION

A significant portion of the crystalline drugs have very low solubilities[1,2] and, consequently, exhibit low bioavailability. This situation has, in turn, led to an increased effort aimed at improving the aqueous solubility of poorly soluble drugs. Since the fundamental physical properties of crystalline material rely upon the molecular arrangement within the solid, therefore, altering the interactions between these molecules directly impacts the physicochemical properties, such as solubility, stability, and bioavailability of crystalline active pharmaceutical ingredients (APIs).[3] One of the current strategies focuses on engineering and screening of crystal phases[4−8] through cocrystal[9,10] or salt[11,12] formation to optimize these properties of APIs.

Lamotrigine (LTG) [3,5-diamino-6-(2,3-dichlorophenyl)-1,2,4-triazine] is an anticonvulsant drug marketed under the brand name Lamictal and is indicated for adjunctive treatment of partial and primary generalized tonic-clonic seizures.[13] It is a BCS class II drug having low solublity in water (0.17 mg/mL at 25 °C),[14] which limits its absorption and dissolution rate in water and thus the bioavailability.[15] LTG is a basic molecule with a diamino-triazine ring having a pK_a of 5.7 at N4 of the triazine ring (Scheme 1). Thus, it has multiple competitive hydrogen-bonding sites, that is, donors and acceptors within its molecular framework, which makes it a potential target for both cocrystal and salt formation studies. Various researchers working on LTG have utilized these strategies of salt,[16−25] solvate,[21,26−32] or cocrystal formation[20,33,34] to improve its

Scheme 1. Molecular Structures of Lamotrigine and All the Coformers Used in This Study

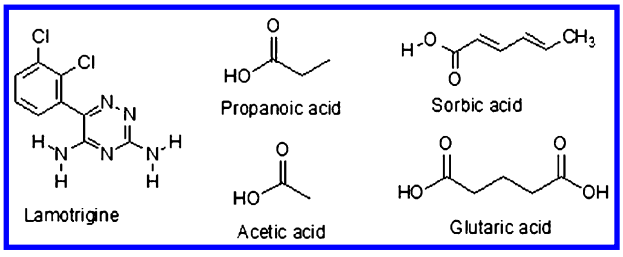

Received: October 23, 2012
Revised: December 25, 2012
Published: January 7, 2013

solubility. The current literature shows that coformers containing carbonyl and amide functionalities are more likely to form cocrystals with LTG, viz. nicotinamide, methylparaben,[20] acetamide,[33] phthalimide, pyromellitic diimide, caffeine, and isophthaldehyde,[34] by hydrogen bonding to its amino groups, whereas all the carboxylic acids tried so far (succinic acid, fumaric acid, tartaric acid,[19] adipic acid, malic acid, nicotinic acid,[20] acetic acid, 4-hydroxybenzoic acid,[33] fluorobenzoic acid, 2-thiobarbituric acid[21]) resulted in the salt formation at the N4 site of LTG. The present work is in continuation with our latest publication[33] on LTG in which we investigated the competing intermolecular interactions between LTG and some pharmaceutically acceptable coformers and subsequent formation of five different muticomponent forms of LTG with nicotinamide (**1**), acetamide (**2**), acetic acid (**3**), 4-hydroxy-benzoic acid (**4**), and saccharin (**5**). It has been learned from the literature[20,33] that LTG multicomponent crystals with disrupted aminopyridine homosynthons may exhibit better solubility profiles in aqueous medium than under acidic conditions. To further understand this correlation between solubility and crystal structures, we searched for more of such LTG crystalline phases by utilizing some selected carboxylic acids having a pK_a value greater than 4 (so that ΔpK_a (pK_a base − pK_a acid) is less than 3) in order to identify any cocrystal formation between LTG and carboxylic acids of higher pK_a values.[5] Four new multicomponent crystal forms of LTG with acetic acid (AA), **6**; propionic acid (PA), **7**; sorbic acid (SA), **8**; and glutaric acid (GA), **9**, are identified, and their complete structural details have been obtained by single-crystal X-ray analysis. Out of these four forms, **6** and **7** have been found to be salts, **8** as a salt-cocrystal, whereas **9** as a salt isobutanolate monohydrate of LTG. The solubility and dissolution properties of these salts and LTG pure base were evaluated in water and 0.1 N HCl, respectively. All four multicomponent forms were found to exhibit higher solubility than the single component parent drug in pure water, but the results were found to be reversed in acidic medium. A correlation of solubility with the crystal packing arrangement has been investigated based upon the type of synthons retained or disrupted in these crystal forms. The stability of the reported forms was also assessed.

EXPERIMENTAL SECTION

Chemicals. LTG was obtained as a complementary sample from Rantus Pharma Pvt. Ltd. (India). The guest compounds and crystallization solvents were of analytical reagent grade and purchased from various commercial suppliers. All of these were used as received.

Sample Preparation. *LTG-Acetic Acid (**6**).* A mixture of LTG (0.256 g, 1 mmol) and AA (0.060 g, 1 mmol) in a 1:1 molar ratio was dissolved in 10 mL of ethyl methyl ketone by heating at 70 °C and stirring to get a clear solution, which was slowly evaporated to get single crystals of **6** that were filtered, air-dried, and stored in a glass vial for analysis. In contrast to the 1:1 stoichiometric ratio of LTG and AA used in preparation of **6**, compound **3** (reported in our previous publication[33]) was obtained by dissolving LTG in an excess of AA. Interestingly, both compounds **3** and **6** are well-reproducible when prepared under controlled solvent conditions.

*LTG-Propionic Acid (**7**).* LTG (0.256 g, 1 mmol) was dissolved in an excess of PA by warming slightly to get a clear solution, which was slowly evaporated to get single crystals of **7** that were filtered, air-dried, and stored in a glass vial for analysis.

*LTG-Sorbic Acid (**8**).* LTG (0.256 g, 1 mmol) was dissolved in a solution of SA in acetone (0.112 g, 1 mmol), and the mixture was stirred at room temperature until a clear solution was obtained, which was then kept at room temperature undisturbed. Single crystals of **8** were obtained overnight, which were filtered, air-dried, and stored in a glass vial for analysis.

*LTG-Glutaric Acid (**9**).* LTG (0.256 g, 1 mmol) was dissolved in a solution of GA in isobutanol (0.067 g, 0.51 mmol). The mixture was stirred and warmed on a water bath until a clear solution was obtained, which was then kept at room temperature undisturbed. Single crystals of **9** were obtained overnight, which were filtered, air-dried, and stored in a glass vial for analysis.

Differential Scanning Calorimetry (DSC). Differential scanning calorimetry analyses of all the samples were conducted using a DSC Q20 (TA Instruments). The samples (3−5 mg) were placed in sealed nonhermetic aluminum pans and were scanned at a rate of 5 °C/min in the range of 25−300 °C under a dry nitrogen atmosphere (flow rate: 50 cc/min). The data were managed by TA Q series Advantage software (Universal Analysis 2000).

Thermogravimetric Analysis (TGA). TGA analyses of all the samples were performed on a Mettler Toledo TGA/SDTA 851e instrument. Approximately 5 mg of each sample was heated from 25 to 300 °C in an open alumina pan at the rate of 10 °C/min under nitrogen purge at a flow rate of 50 cc/min. The data were managed by STAR software (9.00).

Powder X-ray Diffraction (PXRD). PXRD patterns were collected on an X'Pert PRO diffractometer system (Panalytical, Netherlands) with a Cu Kα radiation (1.54060 Å). The tube voltage and current were set at 45 kV and 40 mA, respectively. The divergence slit and antiscattering slit settings were set at 0.48° for the illumination on the 10 mm sample size. Each sample was packed in an aluminum sample holder and measured by a continuous scan between 5 and 50° in 2θ with a step size of 0.017°. The experimental PXRD patterns were refined using X'Pert High Score software.

Fourier Transform Infrared Spectroscopy (FT-IR). A Spectrum RX I FT-IR spectrometer (Perkin-Elmer, U.K.) was employed in the KBr diffuse-reflectance mode (sample concentration: 2 mg in 20 mg of KBr) for measuring IR spectra of the samples over the range of 4000−400 cm^{-1}. Data were analyzed using Spectrum software.

Single-Crystal X-ray Diffraction (SCXRD). X-ray diffraction data set for compound **7** was collected on an Oxford Xcalibur (Mova) diffractometer equipped with an EOS CCD detector and sealed-tube monochromated Mo Kα radiation (λ = 0.71073 Å) at 120 K, whereas X-ray diffraction data sets for compounds **6**, **8**, and **9** were collected on a Bruker AXS Kappa Apex II diffractometer equipped with a CCD detector and sealed-tube monochromated Mo Kα radiation at room temperature (**6**, **8**) and 150 K (**9**). In each case, data were processed and appropriate corrections were made using routine procedures. All structures were solved by direct methods and refined against F^2 using SHELXL-97.[35] Hydrogen atoms in the carboxylic acid groups and amide groups associated with the formation of either a salt or a cocrystal of LTG were located based on the difference Fourier map and were refined isotropically wherever possible. All other hydrogen atoms except those for the water molecule in **9** were placed geometrically and refined with an isotropic displacement parameter fixed at 1.2 times U_q of the atoms to which they were attached. A residual peak of 1.20 e/Å^3 in the final difference Fourier map was located at 1.06 Å away from the H18 atom, indicating no significance to the final structure of **8**. A considerable effort was put to use five different data sets collected at three different temperatures (150−296 K) to improve the refinement results for **9**; however, solvent molecules could best be refined isotropically with reasonable thermal parameters, acceptable metric parameters, and refinement parameters, such as *R*values and insignificant residual electron densities, as reported here. Similarly, a residual peak of 1.168 e/Å^3 in the final difference Fourier map was located at 1.48 Å from the oxygen (O5) atom of isobutanol, indicating no significance to the final structure of **9**. Considering the fact that the OH (O5) group of isobutanol is hydrogen-bonded to the carboxylate oxygen (O1), this peak can be assigned to an oxygen of another water molecule. The WINGX package (version 1.70.01)[36] was used for refinement and production of data tables and ORTEP-3[37] for structural visualization. All ORTEP representations were made using POV-Ray[38] showing ellipsoids at the 50% probability level. Analysis of the H-bonding and other noncovalent interactions was carried out

Table 1. Melting Points and p*K*a Values of LTG and Coformers and the Resulting Δp*K*a Values for the LTG Multicomponent Forms

compound	mp (°C)	pK_a	ΔpK_a (pK_a base − pK_a acid)
LTG (free base)	216−217	5.70	
6	171		
acetic acid	16.64 (mp)[a], 118 (bp)[a]	4.80	0.90
7	175		
propionic acid	−21 (mp)[a], 141 (bp)[a]	4.87	0.83
8	175		
sorbic acid	135	4.76	0.94
9	185		
glutaric acid	97−100	4.34*, 5.22	1.36*

[a]Obtained from Merck Index.

using PARST95 and PLATON[39] for all the structures. Packing diagrams were generated using Mercury-2.3.[40]

Equilibrium Solubility Studies. Equilibrium solubility of LTG free base and all four salts has been determined in water. In each experiment, a flask containing 5 mL of water was equilibrated at 25 °C in a constant temperature bath. An excess of the solid phase was added to the flask, and the resulting slurry was shaken at 200 rpm. An aliquot of slurry was withdrawn after 24 h, filtered through a 0.22 μm membrane filter, and diluted suitably, and the concentration was determined by high-performance liquid chromatography (HPLC). After the last aliquot was collected, the remaining solids were filtered, air-dried, and analyzed by DSC, PXRD, and FT-IR spectroscopy.

Powder Dissolution Studies. For the powder dissolution studies, the starting solids were sieved using a Gilson mesh sieve to provide samples with an approximate particle size of 150 μm. An excess of the solid phase was added to the flask containing 20 mL of 0.1 N HCl maintained at 37 °C, and the resulting slurry was shaken at 200 rpm. An aliquot of slurry was withdrawn at multiple time points up to 6 h, filtered through a 0.22 μm membrane filter, and diluted suitably, and the concentration was determined by HPLC. After the last aliquot was collected, the remaining solids were filtered, air-dried, and analyzed by FT-IR spectroscopy.

HPLC Studies. In the solubility and dissolution experiments on samples of LTG and its salt forms, the solution concentration of LTG was determined by a Waters Alliance HPLC system, which includes a Waters 2695 separation module, a Waters 2996 Photodiode Array Detector, and a 4.6 mm × 150 mm SunFire C18, 5 μm column (Waters Corporation, Milford, MA). Stock standards of LTG for solubility and dissolution studies were prepared by dissolving LTG in 1 mL of methanol and making up the volume with water and 0.1 N HCl, respectively. A 70:30 mixture of phosphate buffer (pH 3.5) and ACN was used to prepare various concentrations of calibration standards in a range of 1000−33 000 ng/mL. Separations of drug and coformers were conducted using the mobile phase of a mixture of phosphate buffer (pH 3.5) and ACN (70:30) pumped at a flow rate of 0.7 mL/min through the column at a temperature of 30 °C. LTG was detected at 265 nm. Data acquisition and analysis were performed using Empower 2.0. software.

Stability Studies. Accurately weighed samples (approximately 100 mg) of pure LTG and its salt forms were placed in loosely capped glass vials and kept in a stability chamber at 40 °C and 75% RH for 1 month and then analyzed by PXRD.

■ RESULTS AND DISCUSSION

The pK_a values of pure drug and coformers used in this study are summarized in Table 1. It is clear from this table that the difference in pK_a values (ΔpK_a) between LTG and the selected carboxylic acids lies in the range of 0−3, thus suggesting the formation of complexes that can be either salts or cocrystals. The molecular structures of all the coformers are given in Scheme 1, and the melting points of complexes along with those of the coformers are given in Table 1.

Thermal Analysis Utilizing DSC and TGA. DSC and TGA scans of LTG and its multicomponent forms are shown in Figures 1 and 2, respectively. The DSC thermogram of LTG

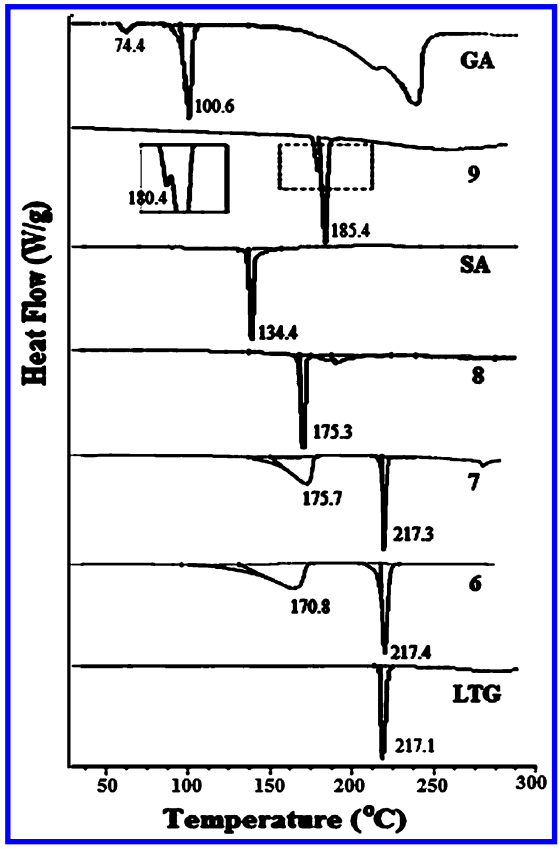

Figure 1. DSC thermograms of LTG free base and its muticomponent forms **6**−**9** along with the coformers used.

showed a single melting endotherm at 217.1 °C, while that of **6** and **7** showed broad endotherms centered at 170.83 and 175.7 °C, respectively, which are accompanied by a weight loss of 17.91% and 22.27%, respectively, in TGA in a temperature range of 130−190 °C, followed by a sharp melting endotherm at 217.3 °C. The broad endotherm indicates the melting of the complexes with simultaneous release of one molecule of AA and PA from the crystal lattice of **6** and **7**, respectively, as suggested by their theoretical weight loss of 18.98% and 22.43%, respectively. Therefore, DSC and TGA results suggest **6** and **7** to be multicomponent crystals of LTG with AA and PA in a 1:1 stoichiometry, respectively. The emergence of a sharp

dx.doi.org/10.1021/cg301556j | Cryst. Growth Des. 2013, 13, 858−870

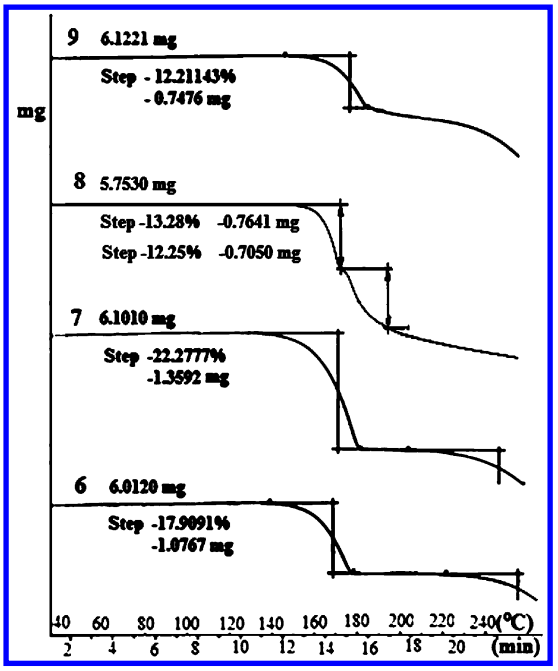

Figure 2. TGA curves of compounds **6**–**9**.

melting endotherm at 217.3 °C suggests the transformation of the original crystal lattice of **6** and **7** to that of pure LTG.

The DSC scan of **8** showed a single, sharp melting endotherm at 175.3 °C that lies in between the melting temperatures of starting components (LTG, 217.1 °C; SA, 134.4 °C), whereas two different endotherms corresponding to the melting point of starting components were observed in the DSC scan of the binary mixture of LTG-SA, thus ruling out the probability of any eutectic formation. Further, no weight loss was observed in TGA of **8** before the final melting of this complex in the range of 160–180 °C, indicating it to be anhydrous and a new stable phase complex of LTG with SA.

The DSC scan of **9** showed an endotherm at 180.4 °C (shown in the inset), followed immediately by another sharp melting endotherm at 185.4 °C. The first endotherm corresponds to desolvation and is accompanied by a weight loss of 12.2% in TGA, which correlates with a theoretical weight loss of 12.5% for desolvation of one molecule of isobutanol and one water molecule from the crystal lattice of **9**, suggesting a stoichiometry of 2:1:1:1 for LTG/GA/isobutanol/H_2O. Immediately after desolvation, the melting of **9** occurs at 185.4 °C. The binary mixture of LTG-GA started melting at 100 °C only (melting point of GA, 100.6 °C), suggesting that peaks appearing in the DSC scan of **9** are not due to any eutectic melting.

Thus, DSC/TGA have shown the existence of multicomponent crystals of LTG with AA, PA, SA, and GA.

PXRD Analysis. All four multicomponent crystals display unique crystalline PXRD patterns in comparison to the starting components, indicating the generation of new solid phases. These unique peaks corresponding to each of the molecular complexes are shown in Figure 3. Thus, the formation of new solid phases in these samples has been identified by a combination of DSC/TGA and confirmed by PXRD analysis; however, the transfer of protons and hydrogen bonding in these solids were ascertained only by FTIR spectroscopy and single-crystal X-ray diffraction studies.

FT-IR Spectroscopy. FT-IR spectroscopy is an excellent technique to characterize and distinguish cocrystals from salts, especially when a carboxylic acid is used as a coformer. LTG shows an IR absorption frequency for a primary amine N–H stretch at 3448 and 3316 cm^{-1}, a C–H aromatic stretch at 3210 cm^{-1}, and a primary amine N–H bend at 1620 cm^{-1} (Figure

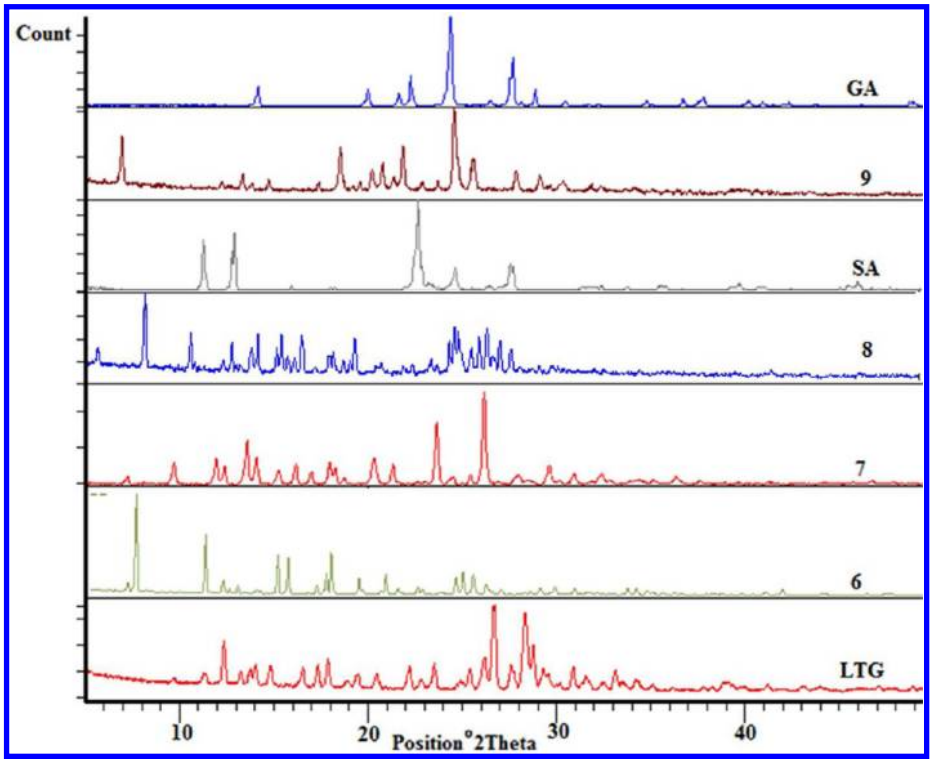

Figure 3. PXRD patterns of LTG free base, coformers, and their multicomponent forms **6**–**9**.

dx.doi.org/10.1021/cg301556j | *Cryst. Growth Des.* 2013, 13, 858–870

4). However, changes were observed in IR peaks of the drug as well as coformers in FT-IR spectra of all four multicomponent

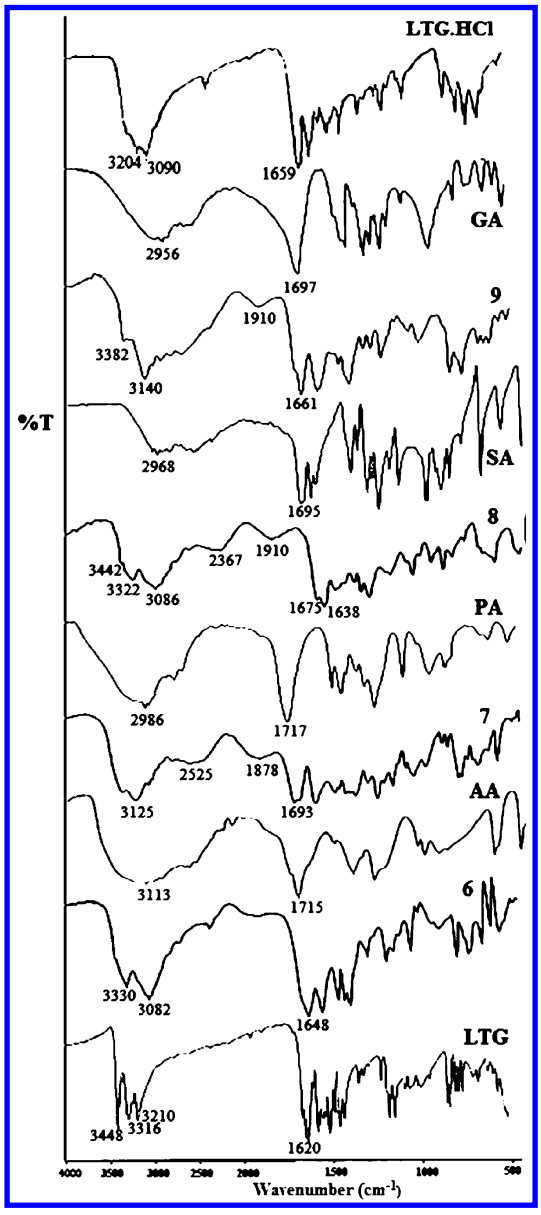

Figure 4. FT-IR spectra of LTG free base, coformers, multicomponent forms **6**–**9**, and LTG hydrochloride salt obtained after dissolution in 0.1 N HCl medium.

forms, which showed characteristic broad bands between 3300 and 1800 cm^{-1} corresponding to $N-H^+$ signals of amine hydrogen-bonded salts (absent in spectra of the drug), suggesting these to be salts of LTG. Further, the shift of the carboxylic acid C=O stretching frequency of AA, PA, SA, and GA from 1715, 1717, 1695, and 1697 cm^{-1} to lower wavenumbers of 1649, 1693, 1675, and 1660 cm^{-1} in IR spectra of **6**, **7**, **8**, and **9**, respectively, clearly indicates the salt formation in these compounds, as the absorption moves to a lower wavenumber if the oxygen atom attached to carbonyl become ionized. Besides this, in the IR spectrum of compound **8**, the primary N–H stretch and N–H bend of LTG is also observed, being shifted from 3448 to 3442 cm^{-1} and from 1620 to 1638 cm^{-1}, respectively. This suggests that, in compound **8**, both the protonated and the neutral LTG molecules are present, which form salts with sorbate ions and cocrystals with neutral SA molecules, respectively. Thus, IR analysis suggests compounds **6**, **7**, and **9** to be salts, whereas **8** to be a salt-cocrystal.

Crystal Structure Analysis. On the basis of the information available in the literature, the crystal structure of LTG is built from hydrogen-bonded dimeric units of the drug molecule showing two dominant supramolecular synthon motifs, the aminopyridine dimer (motif 1) and the amine-aromatic nitrogen synthon (motif 2).[20] However, in all four complexes discussed here, the incorporation of a complementary coformer breaks motif 1 as well as motif 2 (except in complex **8**), but conserves motif 4. The four different hydrogen bond motifs possible for the LTG dimer homosynthon have been represented well in Scheme 2.[33] A proton transfer is also

Scheme 2. All of the Four Hydrogen-Bonding Motifs (Reproduced with Permission from ref 33. Copyright 2011 The Royal Society of Chemistry)

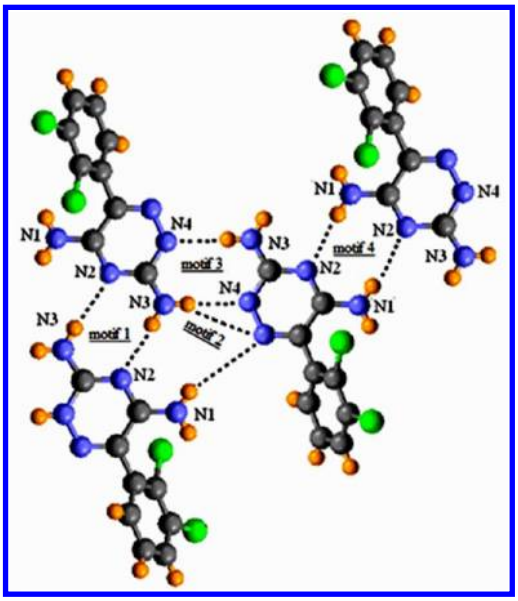

observed from the carboxylic group to the triazine ring of LTG in all the four complexes, as suggested by FT-IR results. Crystallographic data, D_{C-O} distances (i.e., carbon–oxygen distances in the acid carbonyl group), and hydrogen bond geometries of compounds **6**–**9** are given in Tables 2–4, respectively. The comparison of simulated PXRD patterns with the experimental powder patterns showed that the single crystal used to obtain the crystal structure was representative of the bulk of all the samples, except in case of complex **9**, where the correlation is not fairly good, suggesting that the bulk sample of **9** is not very pure (Figure S1, available as Supporting Information).

*LTG-AA Salt, **6** (1:1).* Complex **6** crystallizes in the monoclinic space group $P\bar{1}$, unlike complex **3** (described in our previous publication[33]) that crystallized in the monoclinic space group $P2_1/c$. The asymmetric unit of **3** consisted of one LTG cation and an AA trimer, out of which only one AA molecule transferred its proton to the triazine ring of LTG while the remaining two AA molecules were present in the neutral form, resulting in a 1:3 LTG-AA salt-solvate. In contrast, the asymmetric unit of **6** consists of two LTG cations and two acetate anions (Figure 5). Hence, this complex can be

dx.doi.org/10.1021/cg301556j | Cryst. Growth Des. 2013, 13, 858–870

Table 2. Crystallographic Data for Compounds 6−9

	6	7	8	9
chemical formula	$C_9H_8N_5Cl_2$, $C_2H_3O_2$	$C_9H_8N_5Cl_2$, $C_3H_5O_2$	$C_9H_7N_5Cl_2$, $C_9H_8N_5Cl_2$, $C_6H_7O_2$, $C_6H_8O_2$	$C_{18}H_{16}N_{10}Cl_4$, $C_5H_6O_4$, $C_4H_{10}O_1$, H_2O
stoichiometry	1:1	1:1	1:1:1:1	2:1:1:1
formula wt	316.15	330.17	736.44	736.44
temp (K)	296	120	296	150
wavelength (Å)	0.71073	0.71073	0.71073	0.71073
cryst syst	triclinic	tetragonal	monoclinic	monoclinic
space group	$P\bar{1}$ (No. 2)	$I4_1/a$ (No. 88)	$P2_1/c$ (No.14)	$P2_1/c$ (No. 14)
a (Å)	9.5973(6)	18.6293(4)	9.308(2)	8.8620(6)
b (Å)	11.9400(6)	18.6293(4)	11.356(3)	16.8932(11)
c (Å)	12.7279(6)	17.6086(5)	32.107(8)	22.8226(12)
α (deg)	99.038(4)	90.000(0)	90.000 (0)	90.000(0)
β (deg)	95.005(4)	90.000(0)	96.093(4)	90.170(11)
γ (deg)	90.240(4)	90.000(0)	90.000(0)	90.000(0)
Z	4	16	4	4
vol (Å^3)	1434.67(13)	6111.1(3)	3374.59(13)	3416.7(4)
density (g·cm^{-3})	1.464	1.436	1.450	1.432
μ(mm^{-1})	0.461	0.436	0.403	0.402
F(000)	648	2720	1520	1528
θ (deg) range for data coll.	1.63−25.21	2.70−24.99	1.28−25.10	1.78−25.07
reflns coll.	10 735	16 898	22 805	19 092
independent reflns	5129	2686	5996	5148
reflns with $I > 2\sigma(I)$	2675	1887	3388	2782
R_{int}	0.0397	0.065	0.081	0.0855
no. of params refined	372	195	442	397
GOF on F^2	0.976	1.171	1.044	0.918
final $R_1{}^a$/$wR_2{}^b$ ($I > 2\sigma(I)$)	0.0555/0.1393	0.0508/0.1374	0.0683/0.1626	0.0695/0.1844
weighted R_1/wR_2 (all data)	0.1223/0.1774	0.0786/0.1521	0.1324/0.1987	0.1213/0.2042
largest diff. peak and hole (e·Å^{-3})	0.390 and −0.428	0.531 and −0.366	1.20 and −0.46	1.168 and −0.55

$^a R_1 = \sum||F_o| - |F_c||/\sum|F_o|$. $^b wR_2 = [\sum w(F_o^2 - F_c^2)^2/\sum w(F_o^2)^2]^{1/2}$, where $w = 1/[\sigma^2(F_o^2) + (aP)^2 + bP]$, $P = (F_o^2 + 2F_c^2)/3$.

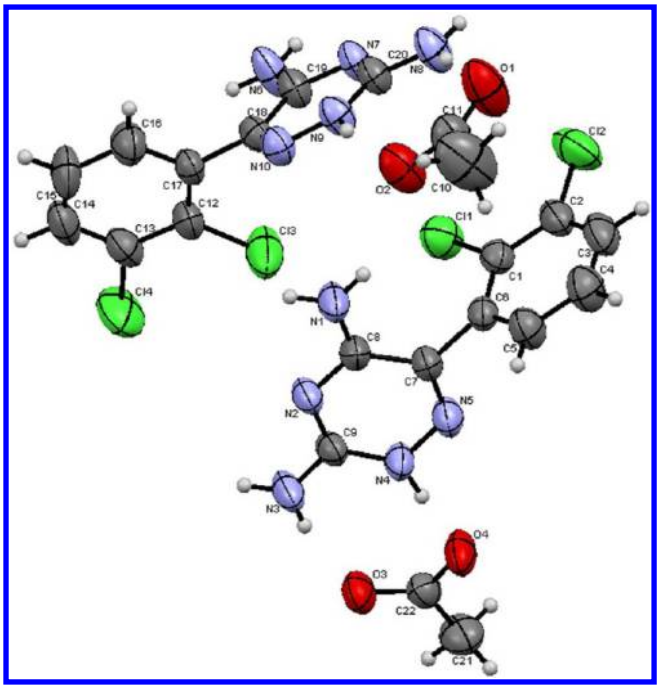

Figure 5. Asymmetric unit of **6**, showing the atom-labeling scheme. Displacement ellipsoids are drawn at 50% probability level.

called a 1:1 salt of LTG and AA. In the crystal lattice of complex **6**, two different LTG dimer homosynthons formed by N−H···N interactions (N6−H6A···N7 and N1−H1B···N2) are present in the *ab* and *bc* planes, respectively, but instead of motif 1 in pure LTG, motif 4 is involved in the formation of both of these dimeric units (Figure 6). In the dimer formed in

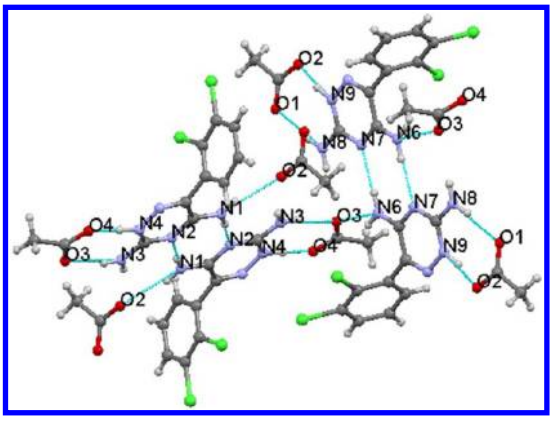

Figure 6. The presence of motif 4 and charge-assisted hydrogen bonding $N^+H\cdots O^-$ and N−H···O in basic supramolecular unit of compound **6**.

the *ab* plane, one LTG molecule is linked to one acetate molecule via $N^+H\cdots O^-$ charge-assisted hydrogen bonding ($N9^+H9A\cdots O2$) and N−H···O interactions (N8−H8A···O1), while the other LTG molecule is linked to one acetate molecule via N−H···O interactions (N6−H6B···O3). Proton transfer is evidenced by the C−O bond distances of the carboxylate group (with ΔD_{C-O} = 0.017 Å; see Table 3) and the geometry of the

dx.doi.org/10.1021/cg301556j | Cryst. Growth Des. 2013, 13, 858−870

Table 3. Distribution of C−O Bond Lengths for Compounds 6−9 Formed with Carboxylic Acids

complex	coformer	D_{C-O} (Å)	ΔD_{C-O} (Å)
6	AA	1.249(6), 1.266(6) (D_{C11-O1}, D_{C11-O2})	0.017
		1.252(5), 1.247(5) (D_{C22-O3}, D_{C22-O4})	0.005
7	PA	1.264(3), 1.258(3) (D_{C10-O1}, D_{C10-O2})	0.006
8	SA	1.211(6), 1.308(6) (D_{C10-O1}, D_{C10-O2})	0.097
		1.266(6), 1.253(5) (D_{C25-O3}, D_{C25-O4})	0.013
9	GA	1.248(6), 1.264(6) (D_{C19-O1}, D_{C19-O2})	0.016
		1.244(6), 1.273(6) (D_{C23-O3}, D_{C23-O4})	0.029

LTG triazine ring. The C20−N9−N10 angle of the triazine ring in the crystal structure of **6** is 121.2(3)°, which correlates well with the previously reported higher values of protonated LTG.[20,41] Similarly, in the dimer formed in the *bc* plane, each LTG molecule is linked to two acetate molecules via $N^+H\cdots O^-$ charge-assisted hydrogen bonding ($N4^+H4A\cdots O4$) and N−H···O interactions (N3−H3A···O3 and N1−H1A···O2). Here also, a proton transfer has occurred, from O4 to N4, as evidenced by the C−O bond distances of the carboxylate group (with ΔD_{C-O} = 0.005 Å) (Table 3) and the C9−N4−N5 angle of the triazine ring (121.3(3)°). Thus, each discrete unit consisting of four LTG molecules and four acetate molecules is linked to four such neighboring units through N−H···N interactions, resulting in formation of a ladder-type network (Figure 7). This structural information correlates well the DSC and TGA results of **6**.

*LTG-PA Salt, **7** (1:1).* Complex **7** crystallizes in the tetragonal crystal system in the centrosymmetric space group $I4_1/a$. Figure 8 shows the asymmetric unit and the atomic numbering scheme. The asymmetric unit consists of one LTG cation and one propionate anion, resulting in a 1:1 salt of LTG and propionic acid. An LTG aminopyridine dimer homosynthon is present in the salt structure (N1−H1A···N2), but instead of N2 and N3 in LTG, N1 and N2 are involved in the formation of the dimeric unit (motif 4). The dimers are further connected to acids through $N^+H\cdots O^-$ charge-assisted hydrogen bonding ($N4^+H4A\cdots O2$) apart from several other N−H···O interactions (N3−H3A···O1, N3−H3B···O1) (Figure 9a). Proton transfer is evidenced by the C−O bond distances of the carboxylate group

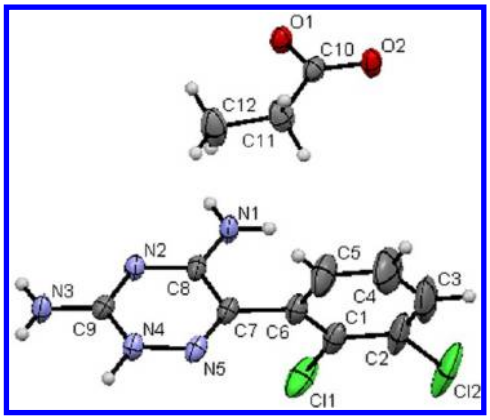

Figure 8. Asymmetric unit of **7**, showing the atom-labeling scheme. Displacement ellipsoids are drawn at 50% probability level.

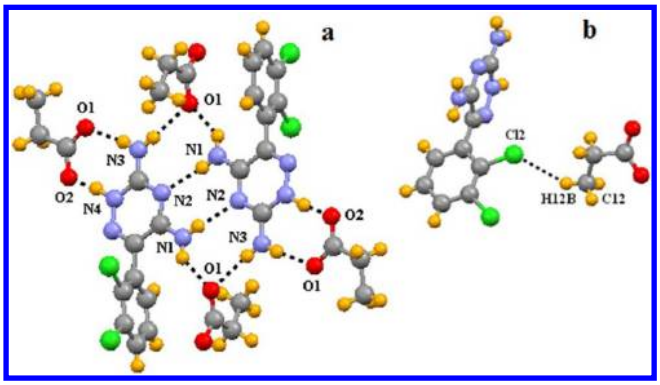

Figure 9. (a) Basic supramolecular unit of **7**. (b) Interactions involving chlorine atoms in compound **7**.

(with ΔD_{C-O} = 0.006 Å) (Table 3) and the angle C9−N4−N5 of the triazine ring (122.8(2)°) of LTG in **7**. The crystal packing is further supported by C−H···Cl hydrogen bonds (C12−H12B···Cl1, C12···Cl1 3.765(4) Å, H12B···Cl1 2.903(1) Å, C12−H12B···Cl1 150.0(2)°) (Figure 9b). Four LTG molecules and four propionic acid molecules altogether form octameric units connected through N−H···O interactions that are responsible for the 4_1 screw symmetry (Figure 10a,b). Thus,

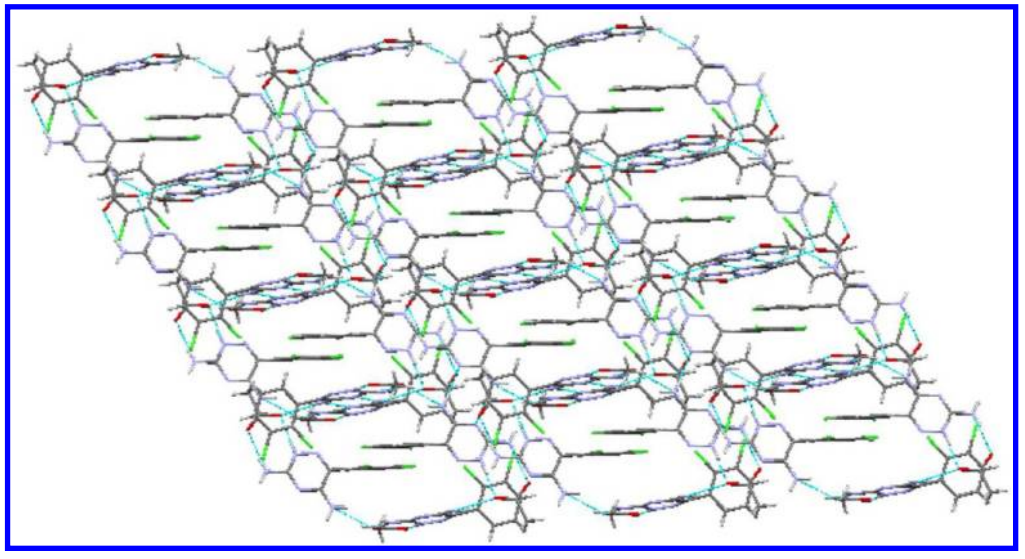

Figure 7. Packing diagram of salt **6** showing the formation of a ladder-type network.

dx.doi.org/10.1021/cg301556j | *Cryst. Growth Des.* 2013, 13, 858−870

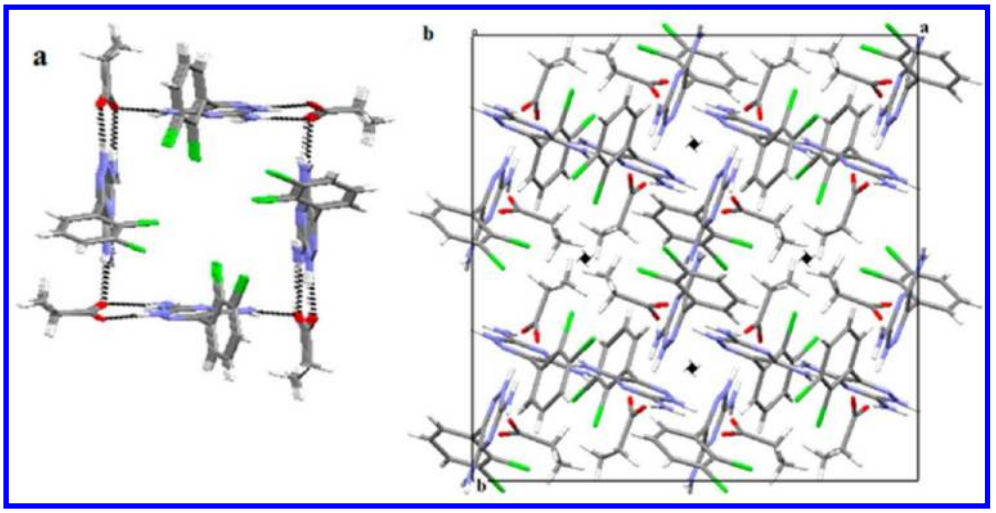

Figure 10. (a) Octameric unit of compound **7** connected through N−H···O hydrogen bonds. (b) The arrangement of molecules around 4_1 screw axis in compound **7** (the white color scheme is used for hydrogen for the packing diagrams for a clear view).

the unusual higher symmetry space group $I4_1/a$ arises for this complex.

*LTG-SA Salt-Cocrystal, **8** (2:2).* Complex **8** crystallizes in the monoclinic space group $P2_1/c$ with an asymmetric unit consisting of a lamotrigine cation and a sorbate anion, along with a neutral LTG and SA molecule (Figure 11). The

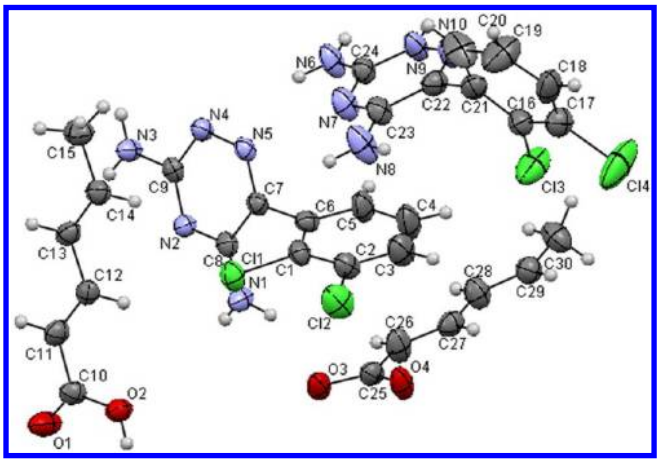

Figure 11. ORTEP diagram of the asymmetric unit of compound **8** with 50% thermal ellipsoid probability.

molecular packing in **8** involves supramolecular heterosynthons formed between the aminopyridinium and carboxylate moieties, through $N^+H\cdots O^-$ charge-assisted hydrogen bonding ($N9^+H9\cdots O4$) and a N−H···O hydrogen bond ((N6−H6B···O3) and between amino and carboxyl moieties through a N−H···O hydrogen bond ((N8−H8B···O4) (Figure 12). This results in forming a supramolecular zigzag-type chain that extends along the *b* axis (Figure 13a). The proton transfer from the carboxylic group (atom O4) to the triazine (atom N9) ring is evidenced by the difference between the C−O bond distances of the carboxylate group (with ΔD_{C-O} = 0.013 Å) (Table 3) and the C18−N9−N10 angle of the triazine ring (122.8(4)°). Another dominant supramolecular synthon present in the crystal lattice of **8** is the LTG dimer, sustained by N−H···N hydrogen bonds (motif 4) (N1−H1B···N2). Both LTG molecules of this dimer are connected to neutral SA molecules through N−H···O hydrogen bonds (N3−H3B···O1)

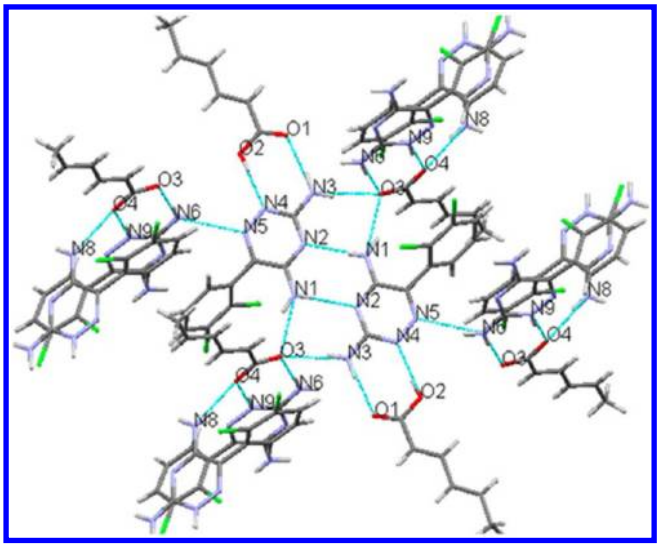

Figure 12. Charge-assisted and neutral hydrogen bonds involved in acid-LTG heterosynthon formation in the basic supramolecular unit of compound **8**.

and O−H···N hydrogen bonds (O2−H2···N4) parallel to the *a* axis (Figure 13b). A ΔD_{C-O} = 0.097 Å for these SA molecules proves them to be present as neutral carboxylic acids (ΔD_{C-O} > 0.08 suggests that carboxylic acid is not ionized, but present in the neutral state), and the C9−N4−N5 angle of 116.4(4)° in the triazine ring of LTG correlates well with that observed for the neutral LTG molecule. This suggests that the LTG molecules involved in the dimer homosynthon (motif 4) are neutral and are hydrogen-bonded to SA molecules, resulting in a 1:1 cocrystal. Each such discrete unit, comprising an LTG dimer hydrogen-bonded to two neutral SA molecules, interacts with four neighboring supramolecular chains of lamotriginium sorbate units running along the *b* axis via N−H···N hydrogen bonds (motif 2) (N6−H6A···N5) and N−H···O hydrogen bonds (N3−H3A···O3), thereby generating a 3D structure. Thus, the overall packing in **8** involves chains formed by lamotriginium sorbate units running along the *b* axis, which are connected by the discrete units of the LTG-SA cocrystal formed along the *a* axis. The structure of **8** thus confirms the

dx.doi.org/10.1021/cg301556j | *Cryst. Growth Des.* 2013, 13, 858−870

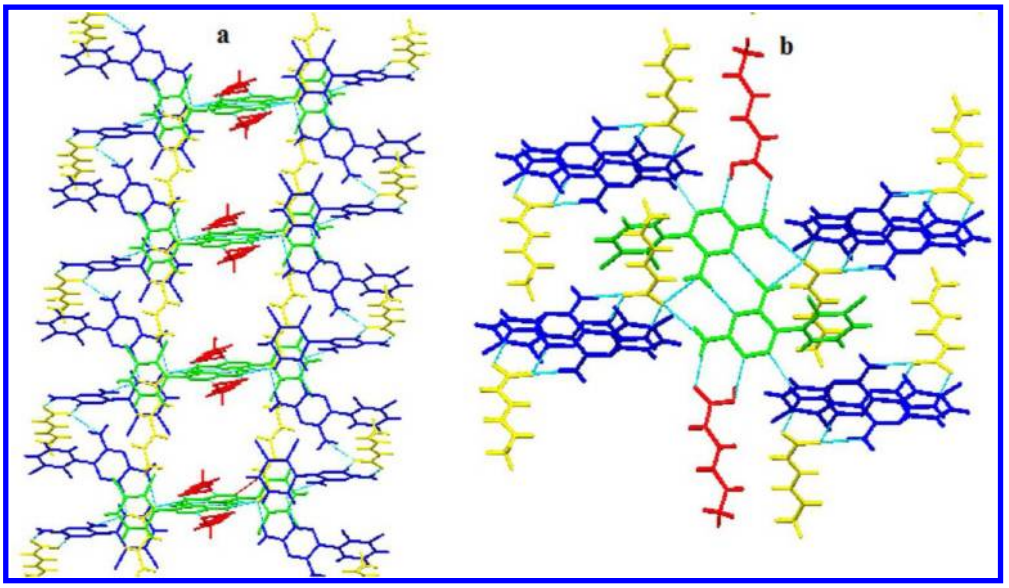

Figure 13. (a) The supramolecular zigzag chains formed by lamotriginium sorbate units running along the *b* axis. (b) LTG dimer sustained by N−H···N hydrogen bonds (motif 4) connected to neutral SA molecules through N−H···O hydrogen bonds and O−H···N hydrogen bonds parallel to the *a* axis (LTG cations, blue; SA anions, yellow; LTG neutral molecules, green; SA neutral molecules, red).

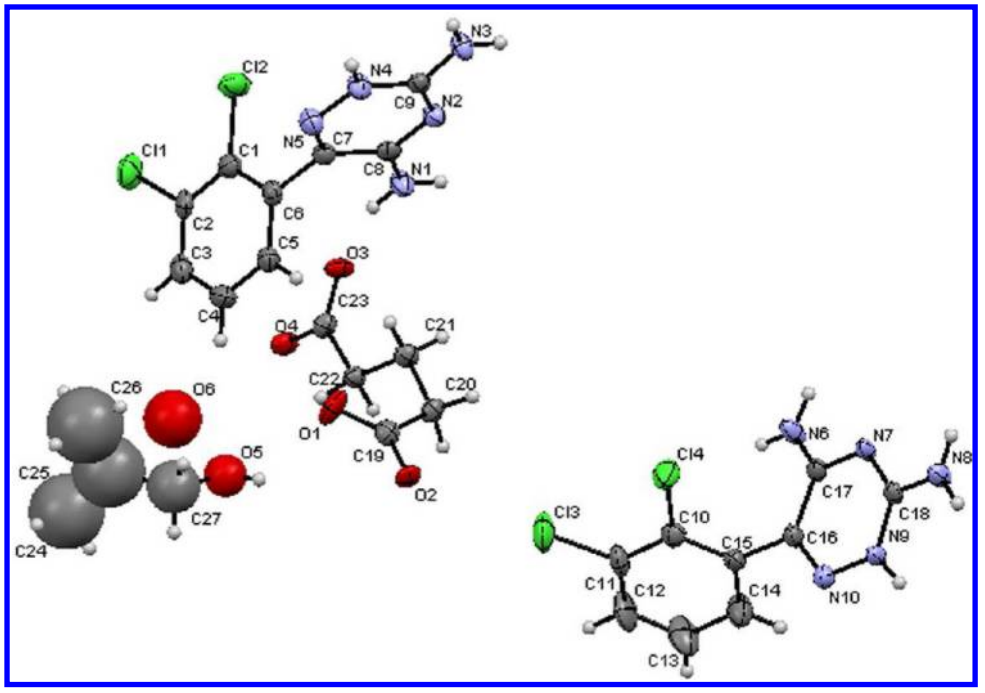

Figure 14. Asymmetric unit of **9**, showing the atom-labeling scheme. Displacement ellipsoids are drawn at 50% probability level.

findings of the FT-IR technique, which suggested the presence of both the salt and cocrystal peaks in the IR spectrum of **8**.

*LTG-GA Salt Isobutanolate Monohydrate, **9** (2:1:1:1).* Complex **9** crystallizes in the space group $P2_1/c$ with the asymmetric unit consisting of two LTG cations, one glutarate dianion, and one molecule each of isobutanol and water (Figure 14). In the crystal lattice of **9**, the LTG molecules form aminopyridine dimers sustained by N−H···N hydrogen bonds (N6−H6C···N7). Interestingly, this dimeric unit involves motif 4, instead of motif 1 found in pure LTG. The homodimers are connected through the GA molecule, thus forming chains extending along the *c* axis. In the chain, one homodimer is connected to the neighboring GA molecules through $N^+H\cdots O^-$ charge-assisted hydrogen bonding ($N9^+H9\cdots O4$) and N−H···O hydrogen bonding (N8H8B···O3), while the next homodimer in the chain is connected to neighboring GA molecules via two-point N−H···O interactions (N6H6D···O2 and N8H8A···O2). The proton transfer from the carboxylic group (atom O4) to the triazine (atom N9) ring is evidenced by the C−O bond distances of the carboxylate group (with ΔD_{C-O} = 0.029 Å) (Table 4) and the C18−N9−N10 angle of the triazine ring in the crystal structure of **9** (122.6(4)°), which correlates with the angle of protonated LTG rather than its neutral form. Further, each LTG homodimer-GA chain is connected to the adjacent chain through GA molecules extending via $N^+H\cdots O^-$ and N−H···O hydrogen bonds. Thus, these drug homodimer-GA

dx.doi.org/10.1021/cg301556j | *Cryst. Growth Des.* 2013, 13, 858−870

Table 4. Geometrical Parameters of Hydrogen Bonds in Compounds 6−9

D−H···A	symmetry	*r* (H···A) (Å)	*r* (D···A) (Å)	*r* (D−H) (Å)	∠D−H···A (deg)
		compound **6**			
N6−H6A···N7	$1-x, 1-y, 2-z$	2.09	2.952(5)	0.86	175(5)
N1−H1B···N2	$2-x, 1-y, 1-z$	2.12	2.974(5)	0.86	174
$N9^{+}$H9A···O2	$-x, 1-y, 1-z$	1.57(6)	2.546(5)	1.00(6)	166(5)
N8−H8A···O1	$-x, 1-y, 1-z$	2.02	2.860(5)	0.86	166
N6−H6B···O3		2.07	2.798(4)	0.86	141
N4+H4A···O4		1.60(5)	2.564(5)	0.97(5)	175(5)
N3−H3A···O3		2.02	2.869(4)	0.86	168
N1−H1A···O2	$1+x, y, z$	2.28	2.999(4)	0.86	141
		compound **7**			
N4−H4A···O2	$x+1, +y, +z$	1.61(3)	2.634(3)	1.03(3)	170(3)
N3−H3A···O1	$x+1, +y, +z$	1.918(2)	2.769(3)	0.860(2)	170.1(2)
N1−H1A···N2	$-x+1/2+1, -y+1/2, -z+1/2+1$	2.074(2)	2.927(3)	0.860(2)	171.1(2)
N1−H1B···O1	$y+1/4, -x+1/4, +z+1/4$	2.109(0.002)	2.790(0.003)	0.860(2)	135.7(2)
N3−H3B···O1	$-y+1/4+1, +x+1/4, -z+1/4+1$	2.117(2)	2.963(3)	0.860(2)	167.8(1)
		compound **8**			
$N9^{+}$H9···O4	$-x, 1/2+y, 1/2-z$	1.79	2.641(6)	0.86	168
N6−H6B···O3	$-x, 1/2+y, 1/2-z$	1.93	2.782(6)	0.86	173
N8−H8B···O4	$1+x, y, -z$	1.97	2.716(6)	0.86	145
N1−H1B···N2	$2-x, 1-y, -z$	2.16(6)	2.924(6)	0.77(6)	176(2)
N3−H3B···O1	$-1+x, y, z$	1.98	2.831(6)	0.86	172
O2−H2···N4	$1+x, y, -z$	1.88	2.665(5)	0.82	161
N6−H6A···N5		2.26	3.021	0.86	148
N3−H3A···O3	$1+x, 1/2-y, -1/2+z$	2.20	3.048	0.86	169
		compound **9**			
N6−H6C···N7	$-x, -y, -z$	2.07	2.931(6)	0.86	179
$N9^{+}$H9···O4	$-1+x, 1/2-y, -1/2+z$	1.78	2.632(5)	0.86	170
N8H8B···O3	$-1+x, 1/2-y, -1/2+z$	1.89	2.750(5)	0.86	173
N6H6D···O2		2.16	2.813(6)	0.86	133
N8H8A···O2	$-x, -y, -z$	2.22	3.006(5)	0.86	152
O5H5A···O1	$1-x, 1/2+y, 1/2-z$	2.26	2.874(8)	0.86	132
$N4^{+}$H4A···O2	$-x, 1/2+y, 1/2-z$	1.89	2.720(5)	0.86	163
N3H3B···O1	$-x, 1/2+y, 1/2-z$	1.95	2.798(6)	0.86	168
N1H1B···O3		1.93	2.744(6)	0.86	157

chains result in formation of sheets diagonal to the *ac* plane (Figure 15). Each GA molecule is also connected to an isobutanol molecule via an O−H···O hydrogen bond (O5H5A···O1) at one carboxyl end and to a water molecule at another carboxyl end with the isobutanol molecules extending out from the plane of sheets.

The molecular packing in **9** also involves another dominant set of supramolecular heterosynthons between the aminopyridinium of LTG and one carboxylate moiety of GA via $N^{+}H\cdots O^{-}$ charge-assisted hydrogen bonding ($N4^{+}$H4A···O2) and N−H···O hydrogen bonding ((N3−H3B···O1). The proton transfer from the carboxylic group (atom O2) to the triazine (atom N4) ring is evidenced by the C−O bond distances of the carboxylate group (with ΔD_{C-O} = 0.016 Å) (Table 4) and the C9−N4−N5 angle of the triazine ring (123.4(4)°). The other carboxylate moiety of this GA molecule is connected to the next LTG molecule through a N−H···O hydrogen bond (N3−H3B···O4), thereby forming chains that run down the *a* axis. These LTG-GA chains are connected to the adjacent chains through a N−H···O hydrogen bond (N1−H1B···O3), thus forming corrugated sheets that extend along the *b* axis in the *ab* plane (Figure 16). These LTG-GA-LTG sheets intersect homodimer-GA-homodimer sheets, thus forming an interwoven three-dimensional network (Figure 17). As a proton transfer is clearly evidenced in both the carboxyl moieties of each GA molecule, this complex can be called a lamotriginium glutarate isobutanolate monohydrate.

The crystal structure of **9** further explains the weight loss step observed in TGA.

Solubility and Powder Dissolution Studies. Equilibrium solubility studies of LTG in its free base sample and all the four multicomponent forms were performed in pure water at 25 °C. Table 5 shows the maximum concentration of drug achieved in the free base sample of LTG and its multicomponent forms. Complexes **6** and **7** have been found to improve the water solubility of LTG by 16 and 14 times, respectively, whereas **8** and **9** improved it up to 7 times that of the free base sample. Interestingly, this increase in water solubility corresponds with decrease in the pH of their solutions in water (which varied due to the presence of acidic coformers in their crystal lattice), as is shown in Table 5. This inverse correlation between solubility and pH in pure water is thus significant in understanding the solubility behavior of complexes reported in this study. The DSC and PXRD analyses (Figures S2 and S3 given in the Supporting Information) of solid residues remaining after the solubility experiment showed that the pure LTG converted to LTG hydrate and the salts **6** and **7** and salt-cocrystal **8** remained almost stable under the aqueous conditions, whereas salt isobutanolate monohydrate **9** transformed to its desolvated salt form.

dx.doi.org/10.1021/cg301556j | *Cryst. Growth Des.* 2013, 13, 858−870

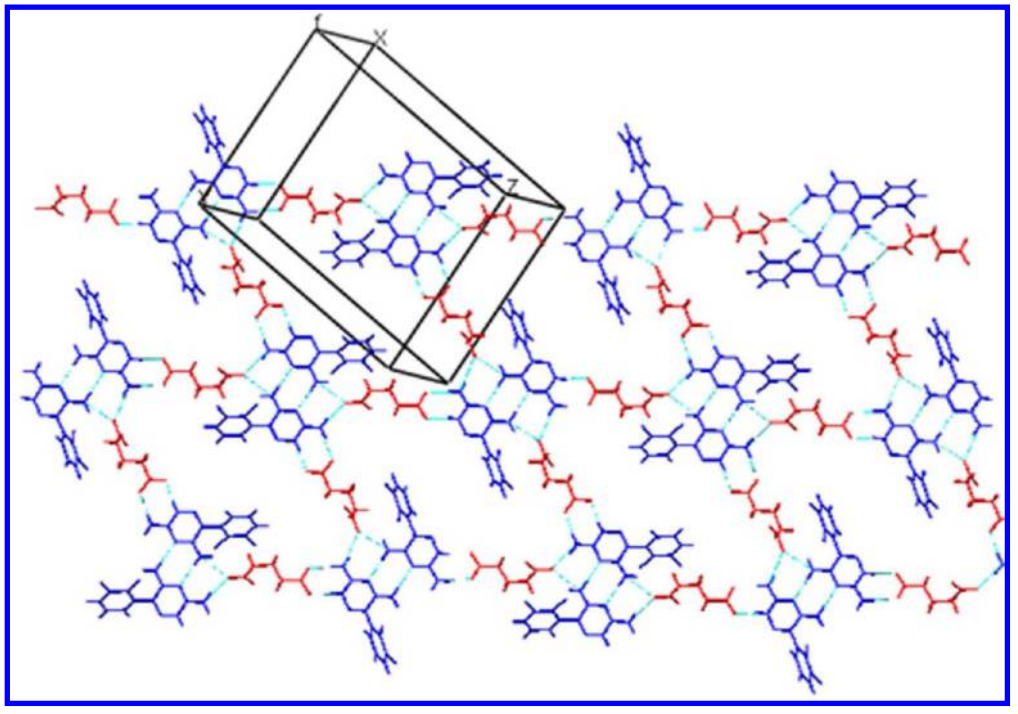

Figure 15. LTG dimer-GA-LTG dimer chains in **9** forming sheets diagonal to the *ac* plane.

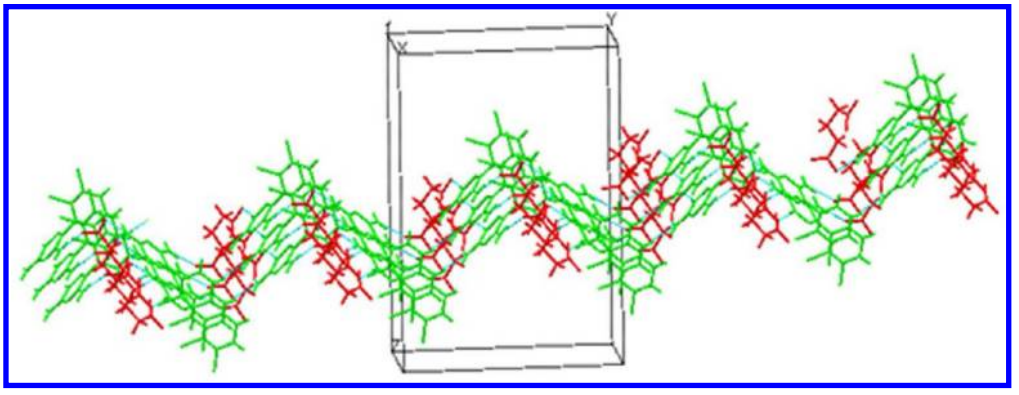

Figure 16. Corrugated sheets formed by LTG-GA chains in **9**, extending along the *b* axis in the *ab* plane.

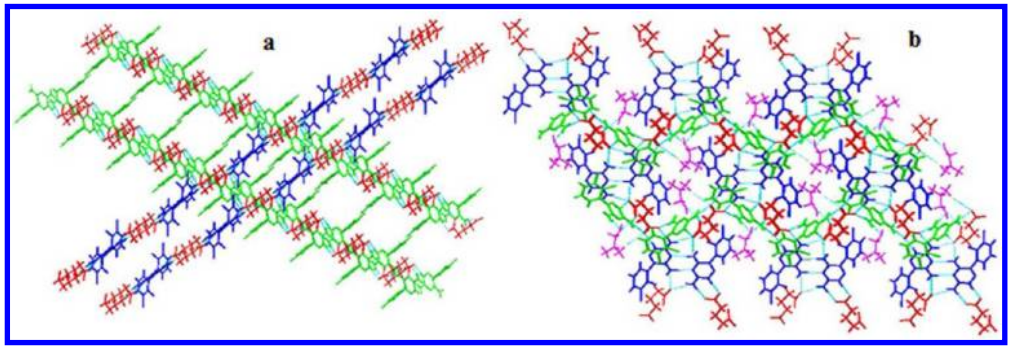

Figure 17. (a) LTG-GA-LTG sheets intersecting LTG dimer-GA-LTG dimer sheets in compound **9**. (b) An interwoven three-dimensional network of compound **9** (LTG cations involved in dimer-GA-dimer sheets, blue; LTG cations involved in LTG-GA-LTG corrugated sheets, green; GA dianions, red; isobutanol molecules, pink; water molecules, yellow).

The dissolution profiles for all the new phases at various time points in 0.1 N HCl at 37 °C are shown in Figure 18 in a comparison to the LTG free base. In the free base sample, LTG reached a maximum concentration of 4.05 mg/mL after a time interval of 25 min, whereas **6**, **7**, **8**, and **9** reached a maximum concentration of 3.12, 3.28, 3.76, and 4.2 mg/mL, respectively, at a time interval of 5 min. After reaching the maximum concentration, the solubility declined slightly before a plateau is achieved. The concentration of the drug achieved in all the salts after 6 h of dissolution study in acidic medium was found to be

dx.doi.org/10.1021/cg301556j | *Cryst. Growth Des.* 2013, 13, 858−870

Table 5. Solubility (mg/mL), pH of Slurry, and Potential Conversion of Multicomponent Forms during Solubility Studies in Water after 24 h at 25 °C

compound	solubility in water at 25 °C after 24 h (mg/mL)	pH of the slurry after 24 h	conversion during experiment[a]
LTG	0.154	6.81	yes (LTG hydrate)
6	2.547	4.91	no
7	2.166	5.01	no
8	1.119	5.06	no
9	1.103	5.15	yes (LTG·glutarate)

[a]Conversion assessed by DSC and PXRD analyses.

lower than that of the free base LTG sample. This can be explained by the fact that, in the case of LTG salts, LTG is already protonated; therefore, lowering the pH of the medium results in decreased solubility of these salts due to the common ion effect. However, among the four multicomponent forms, the salt-cocrystal **8** exhibited the highest stable concentration of LTG during the dissolution studies in acidic medium. The FT-IR analysis of solid residues remaining after the experiment showed that all the samples converted to LTG hydrochloride salt in the HCl medium. The pH of all the solutions resulting after the slurry experiment was also measured, but no significant pH change was observed, suggesting that dissolution profiles in the acidic medium were not affected by the pH.

According to the crystal packing−solubility relationship observed in LTG and its multicomponent forms by Cheney et al,[20] the breaking of motif 2 but retention of motif 1 resulted in improved concentrations of LTG in acidic medium, whereas the breaking of motif 1 increased the concentration in water. The solubility results obtained in the present study are in good agreement with the observations made by Cheney et al.[20] In all the four complexes **6**−**9**, motif 1 is broken, which accounts for their higher solubility in water than the free base LTG. However, the solubility of all of these compounds in acidic medium is lower than that of pure LTG despite the breaking of motif 2 (except **8**, where motif 2 is retained). This can be accounted for by the formation of motif 4 in compounds **6**−**9**. This correlates well with that found in the case of LTG-4-hydroxybenzoate by Chadha et al.,[33] where this compound, possessing motif 4, exhibited lower solubility than pure LTG at pH 2. Thus, it can be inferred that, although the breaking of motif 2 can increase the solubility in acidic medium, the presence of motif 4 lowers the solubility of LTG multicomponent forms in acidic medium. Thus, disruption of motif 1 and formation of motif 4 in compounds **6**−**9** explains their higher solubility in water, but lower solubility in acidic medium, respectively, in comparison with LTG free base.

Stability Studies. The physical stability of LTG free base and its multicomponent forms was investigated at 40 °C/75% RH for 1 month. The DSC and PXRD results showed the total conversion of LTG to LTG hydrate while sample **9** was partially transformed to its desolvated salt form. The PXRD of **6**, **7**, and **8** showed no apparent form change, indicating these to be stable under humid conditions (the post-storage DSC and PXRD results for sample **9** are available as Figures S4 and S5 in theSupporting Information).

CONCLUSION

The work described herein illustrates the complete structural characterization of four new multicomponent forms of LTG that have been identified to be a salt/salt-cocrystal of LTG. The formation of new solid phases in each case was indicated by DSC/TGA and PXRD, whereas the confirmation of the salt/salt cocrystal was performed by FT-IR analysis and single-crystal X-ray diffraction studies. All compounds in this study exhibited the breaking of motifs 1 and 2 that are present in the crystal structure of LTG, but displayed a different motif of the aminopyridine dimer homosynthon (motif 4), except in the case of salt-cocrystal 8, which involved both motifs 2 and 4. This arrangement of packing motifs resulted in a significant improvement in water solubility of complexes **6**−**9**, but lowered their solubility in acidic medium as compared to that of free base LTG. The analysis of solids remaining after the solubility experiment in water and stability studies under high humidity conditions showed that LTG free base converted to its hydrate form and salt isobutanolate hydrate **9** transformed to its desolvated salt form, whereas **6**, **7**, and **8** remained stable even under 100% aqueous conditions. Thus, the work details an effort to prepare and characterize new multicomponent forms of LTG, having better solubility and stability in water than free base LTG.

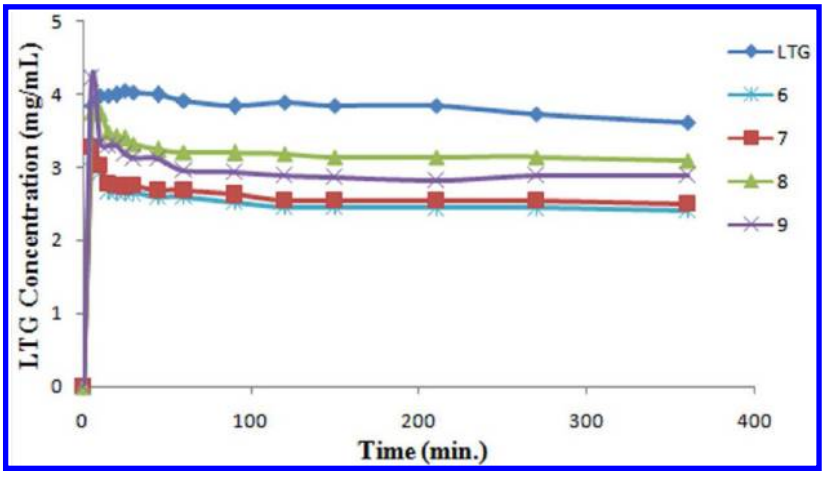

Figure 18. Powder dissolution studies of LTG free base and its multicomponent forms **6**−**9** at various time points in 0.1 N HCl at 37 °C.

dx.doi.org/10.1021/cg301556j | *Cryst. Growth Des.* 2013, 13, 858−870

■ ASSOCIATED CONTENT

Supporting Information

Comparison of experimental PXRD patterns with the simulated patterns, postdissolution DSC and PXRD data, post-storage data for compound **9**, and crystallographic CIF files. This material is available free of charge via the Internet at http://pubs.acs.org. CCDC reference numbers for compounds **6**–**9** are 904852, 821041, 904853, and 904854, respectively.

■ AUTHOR INFORMATION

Corresponding Author

*E-mail: renuchadha@pu.ac.in (R.C.), sanjaymandal@iisermohali.ac.in (S.K.M.). Tel: +91-9316015096 (R.C.), +91-9779932606 (S.K.M.).

Notes

The authors declare no competing financial interests.

■ ACKNOWLEDGMENTS

We gratefully acknowledge the funding provided by the UGC (Research Fellowship for Meritorious Students), New Delhi, India. A.S. and S.K. are grateful to UGC and CSIR, respectively, for research fellowships. The X-ray facility at IISER, Mohali, is gratefully acknowledged.

■ REFERENCES

(1) Amidon, G. L.; Lennernas, H.; Shah, V. P.; Crison, J. R. *Pharm. Res.* **1995**, *12*, 413–420.
(2) Stegemann, S.; Leveiller, F.; Franchi, D.; Jong, H. D; Lindéne, H. *Eur. J. Pharm. Sci.* **2007**, *31*, 249–261.
(3) Walsh, R. D. B.; Bradner, M. W.; Fleischman, S.; Morales, L. A.; Moulton, B.; Rodríguez-Hornedo, N.; Zaworotko, M. J. *Chem. Commun.* **2003**, 186–187.
(4) Vishweshwar, P.; Mcmahon, J. A.; Bis, J. A.; Zaworotko, M. J. *J. Pharm. Sci.* **2006**, *95*, 499–516.
(5) Childs, S. L.; Stahly, G. P.; Park, A. *Mol. Pharmaceutics* **2007**, *4*, 323–338.
(6) Stahly, G. P. *Cryst. Growth Des.* **2007**, *7*, 1007–1026.
(7) Morissette, S. L.; Almarsson, O.; Peterson, M. L.; Remenar, J. F.; Read, M. J.; Lemmo, A. V.; Ellis, S.; Cima, M. J.; Gardner, C. R. *Adv. Drug Delivery Rev.* **2004**, *56*, 275–300.
(8) Chadha, R.; Saini, A.; Jain, D. V. S.; Venugopalan, P. *Cryst. Growth Des.* **2012**, *12*, 4211–4224.
(9) Bethune, S. J.; Schultheiss, N.; Henck, J. *Cryst. Growth Des.* **2011**, *11*, 2817–2823.
(10) Yan, Y.; Chen, J.; Geng, N.; Lu, T. *Cryst. Growth Des.* **2012**, *12*, 2226–2233.
(11) Martins, F. T.; Bonfilio, R.; Araujo, M. B. D.; Ellena, J. *J. Pharm. Sci.* **2012**, *101*, 2143–2154.
(12) Sanphui, P.; Bolla, G.; Nangia, A. *Cryst. Growth Des.* **2012**, *12*, 2023–2036.
(13) Perucca, E. *Clin. Pharmacokinet.* **2000**, *38*, 191–204.
(14) *The Internet Drug Index*. Available at: www.rxlist.com/cgi/generic/lamotrigine.htm (accessed Nov 13, 2009).
(15) Parmar, K. R.; Patel, K. A.; Shah, S. R.; Sheth, N. R. *J. Inclusion Phenom. Macrocyclic Chem.* **2009**, *65*, 263–268.
(16) Sawyer, D. A.; Copp, F. C. U.S. Patent 4,847,249, 1989.
(17) Potter, B.; Palmer, R. A.; Withnall, R.; Leach, M. J.; Chowdhry, B. Z. *J. Chem. Crystallogr.* **1999**, *29*, 701–706.
(18) Sridhar, B.; Ravikumar, K. *Acta Crystallogr.* **2009**, *C65*, o460–o464.
(19) Galcera, J.; Molins, E. *Cryst. Growth Des.* **2009**, *9*, 327–334.
(20) Cheney, M. L.; Shan, N.; Healey, E. R.; Hanna, M.; Wojtas, L.; Zaworotko, M. J.; Sava, V.; Song, S.; Sanchez-Ramos, J. R. *Cryst. Growth Des.* **2010**, *10*, 394–405.
(21) Sridhar, B.; Ravikumar, K. *J. Chem. Crystallogr.* **2011**, *41*, 1289–1300.
(22) Rahman, Z.; Zidan, A. S.; Samy, R.; Sayeed, V. A.; Khan, M. A. *AAPS PharmSciTech* **2012**. DOI: 10.1208/s12249-012-9800-9.
(23) Galcera, J.; Friscic, T.; Hejczyk, K. E.; Fabian, L.; Clarke, S. M.; Day, G. M.; Molins, E.; Jones, W. *CrystEngComm* **2012**, *14*, 7898–7906.
(24) Razzaq, S. N.; Khan, I. U.; Sahin, O.; Buyukgungor, O. *Acta Crystallogr.* **2010**, *E66*, o2558.
(25) Qian, Y.; Lv, P.; Shi, L.; Fang, R.; Song, Z.; Zhu, H. *J. Chem. Sci.* **2009**, *121*, 463–470.
(26) Sridhar, B.; Ravikumar, K. *Acta Crystallogr.* **2005**, *E61*, o3805–o3807.
(27) Janes, R. W. *J. Chem. Crystallogr.* **1999**, *29*, 163–167.
(28) Parthasaradhi, R. B.; Rathnakar, R. K.; Raji, R. R.; Muralidhara, R. D.; Chander, R. K. S. U.S. Patent 2005/0119265 A1, 2005.
(29) Sridhar, B.; Ravikumar, K. *Acta Crystallogr.* **2006**, *E62*, o4752–o4754.
(30) Janes, R. W.; Lisgarten, J. N.; Palmer, R. A. *Acta Crystallogr.* **1989**, *C45*, 129–132.
(31) Kubicki, M.; Codding, P. W. *J. Mol. Struct.* **2001**, *570*, 53–60.
(32) Sridhar, B.; Ravikumar, K. *Mol. Cryst. Liq. Cryst.* **2007**, *461*, 131–141.
(33) Chadha, R.; Saini, A.; Arora, P.; Jain, D. V. S.; Dasgupta, A.; Guru Row, T. N. *CrystEngComm* **2011**, *13*, 6271–6284.
(34) Leksic, E.; Pavlovic, G.; Mestrovic, E. *Cryst. Growth Des.* **2012**, *12*, 1847–1858.
(35) Sheldrick, G. M. *Acta Crystallogr.* **2008**, *A64*, 112–122.
(36) Farrugia, L. J. *J. Appl. Crystallogr.* **1999**, *32*, 837–838.
(37) Farrugia, L. J. *J. Appl. Crystallogr.* **1997**, *30*, 565.
(38) *POV-Ray*, version 3.6; Persistence of Vision Raytracer Pty. Ltd.: Victoria, Australia, 2003–2009.
(39) Spek, A. L. *J. Appl. Crystallogr.* **2003**, *36*, 7–13.
(40) Macrae, C. F.; Bruno, I. J.; Chisholm, J. A.; Edgington, P. R.; McCabe, P.; Pidcock, E.; Rodriguez-Monge, L.; Taylor, R.; Streek, J. V. D.; Wood, P. A. *J. Appl. Crystallogr.* **2008**, *41*, 466–470.
(41) Palmer, R.; Potter, B.; Leach, B. M.; Chowdhry, B. *J. Chem. Crystallogr.* **2007**, *37*, 771–777.